Journal of Crystal Growth 112 (1991) 635–643
North-Holland

A transmission and high-resolution electron microscope study of cozonally twinned growth of eutectic silicon in unmodified Al–Si alloys

M. Shamsuzzoha

Department of Materials Science and Engineering, University of Arizona, Tucson, Arizona 85721, USA

L.M. Hogan

Department of Mining and Metallurgical Engineering, University of Queensland, St. Lucia, Brisbane, Queensland 4067, Australia

David J. Smith

Center for Solid State Science and Department of Physics, Arizona State University, Tempe, Arizona 85287, USA

and

P.A. Deymier

Department of Materials Science and Engineering, University of Arizona, Tucson, Arizona 85721, USA

Received 27 July 1990; manuscript received in final form 5 February 1991

The crystallography of the silicon phase in unmodified Al–Si eutectic alloys has been studied by conventional and high-resolution electron microscopy. Examination of the flake morphology eutectic silicon, at two mutually perpendicular ⟨110⟩ zone axes, revealed internal twin traces at only one ⟨110⟩ zone axis, parallel to the flake surface. Internal twins in the silicon phase appear to develop as a result of purely two-dimensional crystal growth on pre-existing silicon nuclei containing a group of parallel twins. The twins grow along coplanar ⟨112⟩ directions by the twin plane re-entrant edge (TPRE) mechanism. Stacking faults and twins present in the high-resolution images of eutectic silicon are consistent with TPRE growth originating at the silicon nuclei containing parallel twins.

1. Introduction

The eutectic silicon in unmodified Al–Si alloys frozen at moderate rates as in sand-casting tends to assemble in the form of branched clusters of plates or flakes often referred to as a wheatsheaf configuration (fig. 1). Individual flakes in such an assembly exhibit internal {111} twins [1]. Previous TEM diffraction studies [2–4] on directionally growing Al–Si eutectic microstructures have firmly established a two-dimensional crystal morphology for flake-type silicon, as shown in fig. 2. The flake exposes its {111} surface to the adjacent eutectic aluminium phase. The parallel {111} twins within the flake produce a stable 141° re-entrant groove also faced by {111} planes at the growth tip. The groove is efficient in retaining silicon atoms deposited from the melt and promotes faster growth along ⟨112⟩. This crystal growth behavior conforms well with the twin plane re-entrant edge (TPRE) growth mechanism [5,6].

The branched clusters in fig. 1 occur repetitively during growth of the unmodified eutectic. As the flakes diverge, a cluster becomes unstable

0022-0248/91/$03.50

and is replaced by a new cluster expanding from a point. Between the clusters relatively disordered groups of platelets occur, as visible at top left in fig. 1. Within a cluster, each plate grows in a ⟨112⟩ direction, as shown in fig. 2f, in conformity with the TPRE growth mechanism, and all active {111} twin planes in the cluster are coplanar, i.e., all are parallel to a single ⟨110⟩ zone axis.

In any monocrystalline platelet, four {111} planes are available for twinning, but evidence suggests [2–4] that twinning occurs on only one set of coplanar {111} planes in any one radiating cluster. This exclusive behavior continues when branching occurs. There is no obvious reason why twins should not form on the three apparently inactive planes, especially since it is known that, in the presence of strontium or sodium modifiers, all four planes are highly active [7,8]. Further diffraction studies to search for twins on the apparently inactive {111} planes were therefore considered desirable. A modified TEM technique was used and, as a further aid to understanding the growth mechanism at the atomic level, high-resolution electron microscopy (HREM) was also employed.

2. Experimental procedures

Alloys of eutectic composition (12.7 wt% Si) were vacuum cast from aluminium and silicon each of 99.999% purity. The cast billets were swaged to 5 mm or less diameter rods and then remelted and unidirectionally solidified at rates of 50 to 250 μm s^{-1}. The thermal gradient at the solid–liquid interface was determined to be 50 °C cm^{-1} by prior calibration of the furnace apparatus. Longitudinal and transverse section specimens taken from near the center of the solidified samples were used for scanning electron microscopy (SEM) and thin film preparation. The thin foil specimens were prepared by a method described elsewhere [3], using electropolishing followed by ion beam thinning.

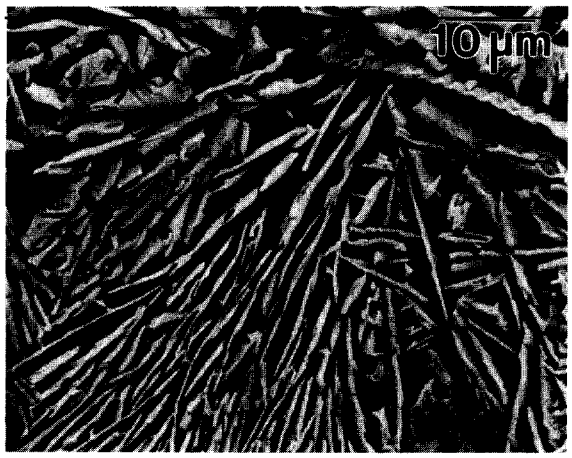

Fig. 1. SEM micrograph showing a typical wheatsheaf cluster of silicon in Al–Si eutectic, Al–12.7%Si, sand cast.

The thin foils were examined with a Philips EM-400T and a 400 kV JEM-4000EX electron microscope. In both microscopes, the specimens were usually tilted to align a ⟨110⟩ zone axis projection of the silicon flakes with the direction of the electron beam. High-resolution electron micrographs were recorded near the optimum defocus typically at a magnification of 500,000 ×. The atomic columns appear black under these experimental conditions and the structure of twin boundaries and other defects could be resolved unambiguously.

3. Experimental results

The microstructure of the silicon phase was investigated three-dimensionally by the convergent beam electron diffraction (CBED) technique. After locating a suitable silicon flake in the microscope, a convergent beam of probe diameter less than 100 nm was selected to obtain relevant diffraction information. The convergent electron beam in conjunction with a reduced diffraction volume of the silicon phase yielded well-defined Kikuchi-line patterns. Using the goniometer tilting facilities in the microscope, the orientation of the selected silicon flake was shifted to two mutually perpendicular ⟨110⟩ zone axes.

3.1. Three-dimensional geometry of eutectic silicon

Bright field micrographs from a single silicon flake taken at two mutually perpendicular ⟨110⟩ zones axes, namely [$\bar{1}$10] and [110], are shown in

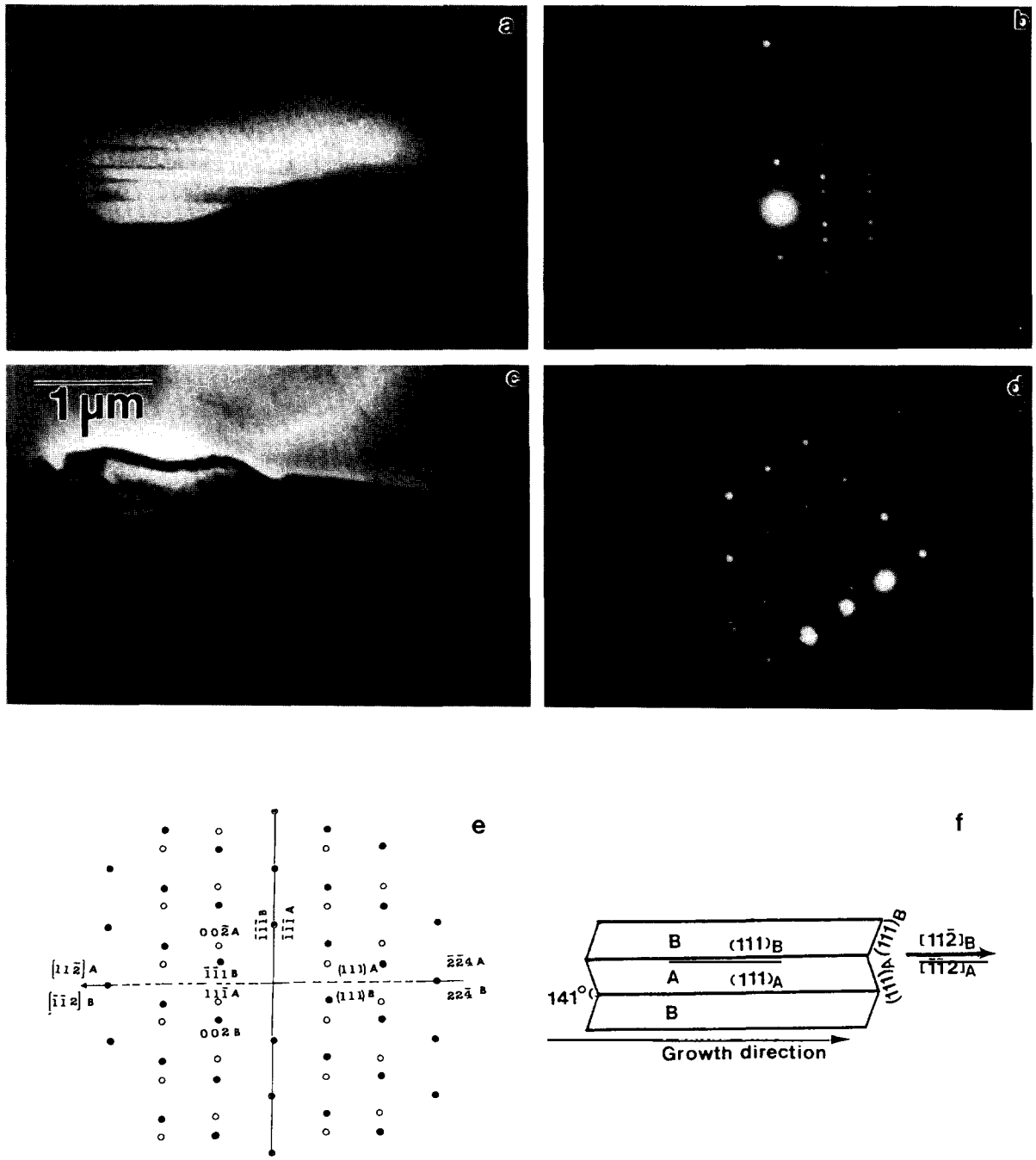

Fig. 2. TEM micrographs and electron diffraction patterns illustrating the presence of twinning on one set of {111} Si planes. Al–12.7%Si; $v = 89\ \mu m\ s^{-1}$; $G = 50\,^{\circ}C\ cm^{-1}$; (a), (c) bright-field electron micrographs of the same Si flake with electron beam parallel to two different ⟨110⟩ directions; (b), (d) electron diffraction patterns from the Si flake corresponding to (a) and (c); respectively; (e) indexing of diffraction spots in (b); (f) orientation relationships for the twinned Si flake in (a), typical for TPRE growth.

figs. 2a and 2c. Corresponding diffraction patterns are given in figs. 2b and 2d. The presence of parallel twin traces on a single {111} plane separated by distances on the order of microns, as in fig. 2a, and paired diffraction spots due to twinned orientations in the corresponding diffraction patterns (see fig. 2b), clearly indicates that in the $[\bar{1}10]$ orientation of the silicon flakes only one of the two cozonal {111} planes is twinned, as shown in fig. 2e. By contrast, the bright field image of the same flake, and its corresponding electron diffraction pattern (fig. 2d), taken at the [110] zone axis, show no evidence for such twinning characteristics, indicating that all {111} planes cozonal to this ⟨110⟩ zone axis are twin-free.

In any cubic crystal, the $[\bar{1}10]$ and [110] zone axes are cozonal to four independent {111} planes. The present microscope observations strongly suggest that, amongst all four possible {111} planes of the silicon flake, only one is twinned. The {111} twins in the silicon flake could form either during crystal growth or else result from deformation caused by the different thermal expansion of the eutectic species. The latter seems possible since silicon is known to have a smaller coefficient of thermal expansion than aluminium and is more likely than aluminium to be in compression. However, for a very thin long cylindrical rod embodied in the matrix of another media, the compressive stresses due to thermal expansions are axissymmetric. This means that shear stresses τ_{RZ} and τ_{ZR} (where R and Z are the radius and axial direction of the cylindrical rod, respectively) are the only shear stresses operative on the cylinder and they were found to be zero on the principal planes of the cylinder [9]. Thus, ignoring the effect of anisotropy for a silicon flake in the aluminium matrix, the shear stress will be zero on {111} planes parallel to the flake axis. The presence of cozonal {111} twins parallel to flake surfaces of silicon as well as the stress analysis argument indicates that twins or other {111} faults must be inherent to the growth of the silicon flake. These defects are thus responsible for the ⟨112⟩ growth. The three-dimensional geometry of a silicon flake tip needed to acquire silicon atoms from the melt for crystal growth is therefore identical to that determined in previous TEM studies (fig. 2e). In other words, the growth of the silicon phase in unmodified Al–Si alloys is purely two-dimensional.

At the solid–liquid interface, the growth tip of silicon exposes only cozonal {111] surfaces to the eutectic melt. Upon freezing, the local diffusion conditions of the eutectic melt constrain the growth of the silicon phase to continue either uninterrupted along the flake axis or at the particular angle from the flake axis required to maintain near constant interphase spacing. In either case, the twinning required for the ⟨112⟩ TPRE growth involves only cozonal {111} planes. This forces the TPRE growth to proceed only along those ⟨112⟩ directions which are coplanar with the {111} twining planes. The mechanisms for the growth direction change of eutectic silicon are discussed in detail elsewhere [7]. Figs. 3 and 4 show two very good examples of such growth direction changes observed in silicon flakes. The interconnected silicon flakes in each case exhibit {111} twin traces at a single orientation suggesting that all {111} twin planes responsible for the TPRE growth along various ⟨112⟩ directions are cozonal. The dark field micrographs recorded using the corresponding twinned diffraction pattern spots also showed that the constituent twins were cozonal. Moreover, no non-cozonal twin which could initiate nonplanar ⟨112⟩ TPRE growth was found in any individual silicon flakes present in these branched assemblies.

3.2. Atomic level structure of eutectic silicon

In a ⟨110⟩ projection of the diamond cubic structure of silicon, with cell parameter $a = 0.543$ nm, the interplanar spacings for the {110}, {111} and {400} planes are 0.384, 0.313 and 0.138 nm, respectively. The latter lies below the resolution limit of the 400 kV HREM and cannot be resolved in high-resolution micrographs. The HREM image observed for a ⟨110⟩ projection of the diamond cubic structure of silicon is thus identical to that observed for an fcc crystal with similar cell dimensions. This limitation, however, does not produce any change in the symmetry of defects [10] such as {111} twins, {111} stacking faults and twin boundary dislocations observed in HREM images, and therefore does not preclude the analysis of such defects.

Fig. 5 shows an HREM image of a silicon flake segment taken with the electron beam aligned with a ⟨110⟩ direction of the flake. The image shows parallel twin boundaries with the same {111} plane and extending along a ⟨112⟩ direction. The twin structure can be recognized in the magnified HREM image (fig. 5b) from the fact that, across the twin plane, the –abcabc– {111} atomic stacking of the diamond cubic structure is replaced by the stacking sequence –abcba– (fig. 5c), in which the c plane, designated as T in the micrograph of fig. 5b, acts as the twin plane. This configuration of twin structures labelled as A, B in the flake segment of figs. 3a and 3b follows the pattern of fig. 2f and, therefore, conforms well with the TPRE growth mechanism established by the previous TEM studies.

In addition to twins, the high-resolution electron micrograph of fig. 5a shows a {111} stacking fault, designated as SF, which also runs parallel to

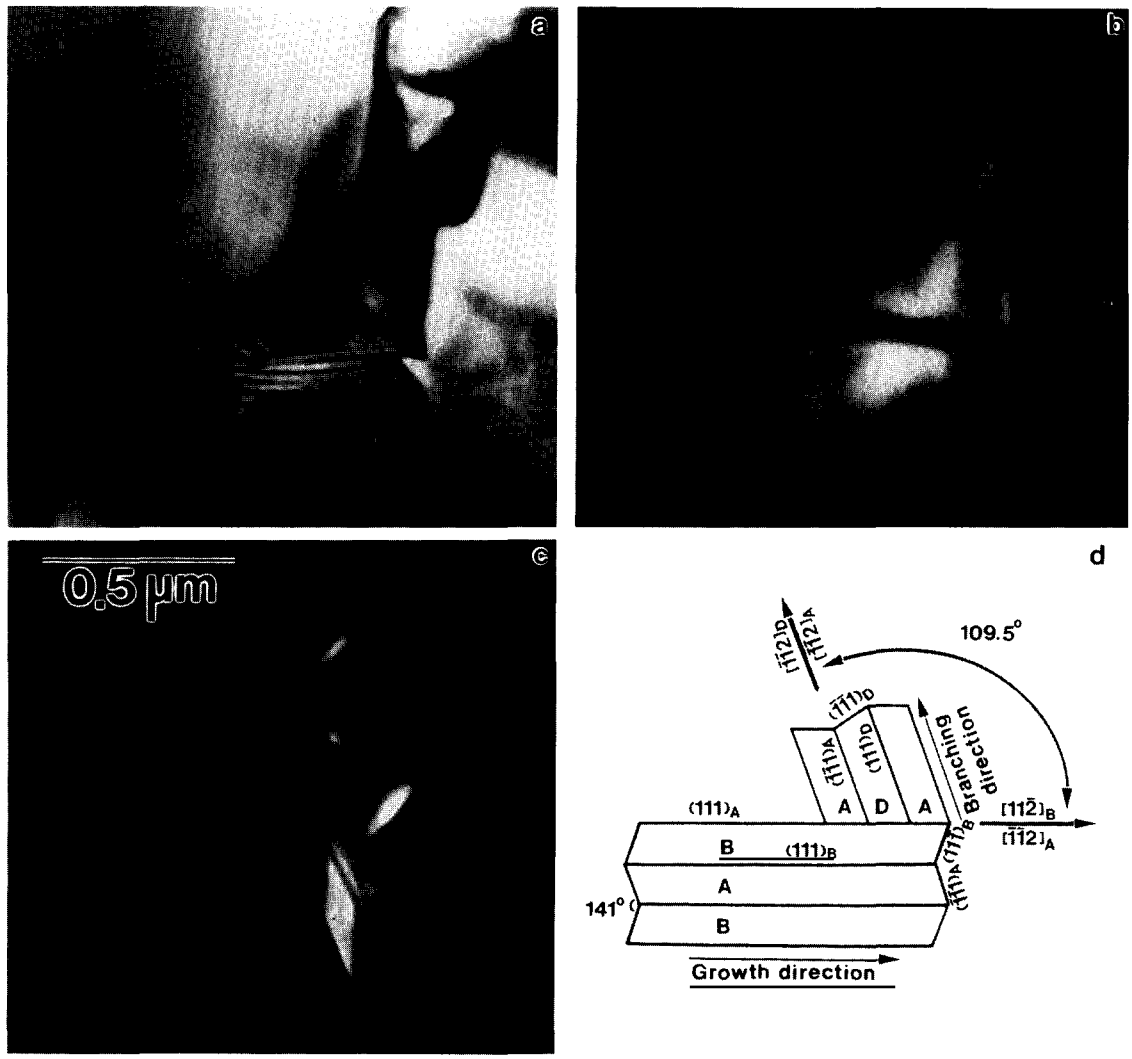

Fig. 3. TEM micrographs, longitudinal section, 109.5° branching of eutectic Si: Al–12.7%Si; $v = 250\ \mu m\ s^{-1}$; $G = 50\,^{\circ}C\ cm^{-1}$; (a) bright-field, inverted L-shape Si at the center; (b), (c) dark-field, showing twin orientations; (d) schematic of orientation relationships between twinned crystals forming a 109.95° branching.

the twin plane. In the magnified image (fig. 5b), the atomic structure of the faulted region is well-resolved. In this region, the local {111} stacking sequence exists in the form of –abab– (fig. 5d), indicating that it is an intrinsic stacking fault. The continuation of the stacking fault over the entire length of the silicon flake in conjunction with its rare occurrence seems to indicate that this fault was probably not produced as a result of any irregularity in the deposition of silicon atoms from the melt to the growth tip. Rather, it is more likely to be a random growth fault which occurred during the nucleation stage of the silicon flake.

The atomic structure of the matrix silicon in the HREM micrograph is remarkably free of any line defects and is typical of that observed with the dislocation density of $10^8\,cm^{-1}$ found in solidified materials. The majority of the defects found were concentrated at the twin boundaries. Fig. 6a shows such a line defect present at the position marked A at the twin boundary. A Frank dislocation circuit (fig. 6b) applied to the defect gives a

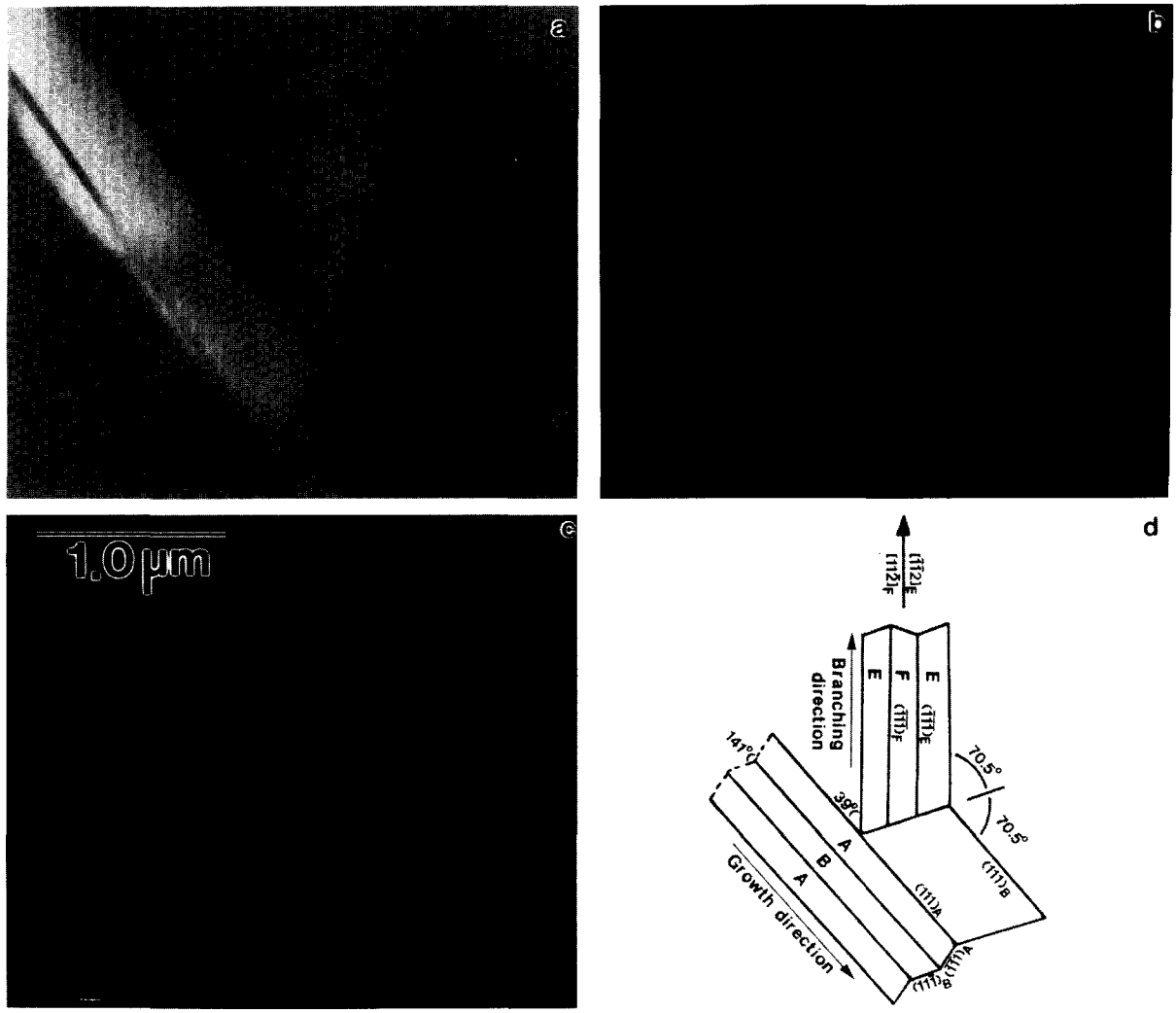

Fig. 4. TEM micrographs, longitudinal section, 39° branching of eutectic Si. Al–12.7%Si; $v = 50\ \mu m\ s^{-1}$; $A = 50\,°C\ cm^{-1}$; (a) bright-field, T-shaped Si at the center; (b), (c) dark-field, showing twin orientations; (d) schematic of orientation relationships between twinned crystals forming a 39.0° branching.

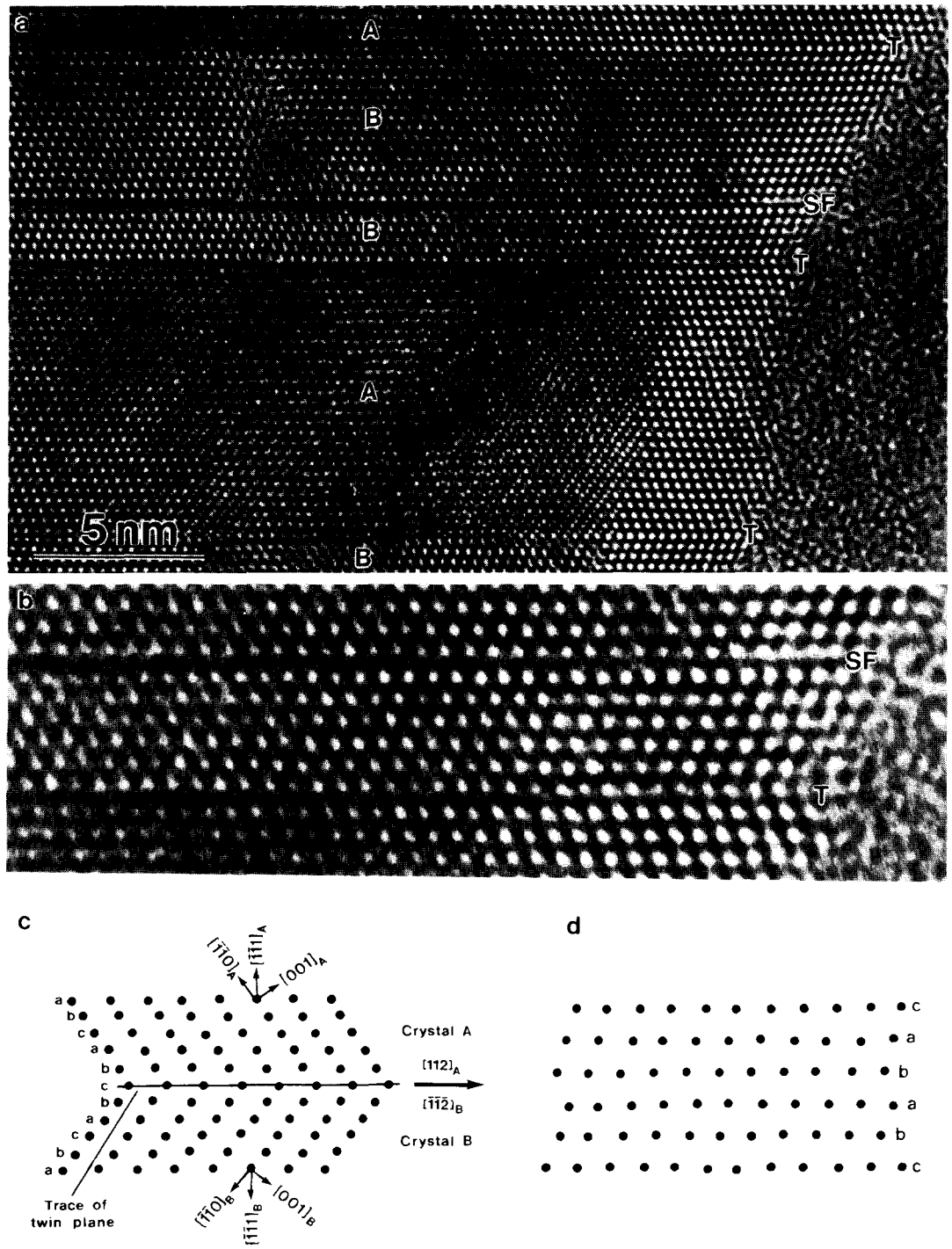

Fig. 5. (a) High-resolution electron micrograph of Si flake with twins (marked T) and intrinsic stacking fault (SF); (b) magnified image from (a) showing stacking fault (SF) and twin (T); (c) schematic showing atomic stacking at twin plane; (d) schematic of intrinsic stacking fault.

closure failure vector of magnitude $\frac{1}{3}$ [$\bar{1}$11] for the dislocation associated with this line defect. This circuit is a projection on the plane of the micrograph and obviously does not provide information about out-of-plane components of the closure failure vector. However, the most plausible defect showing the observed closure failure is a secondary grain boundary dislocation predicted [11] on the basis of various geometrical models of grain boundaries [11–14]. According to these geometrical models, when a grain boundary deviates from its ideal orientation at some position along its length, a secondary grain boundary dislocation forms in the immediate vicinity of the defective boundary in order to accommodate the local deviation. In the presence of the extra half-plane associated with such a dislocation, the boundary conserves its continuity with an ideal orientation after

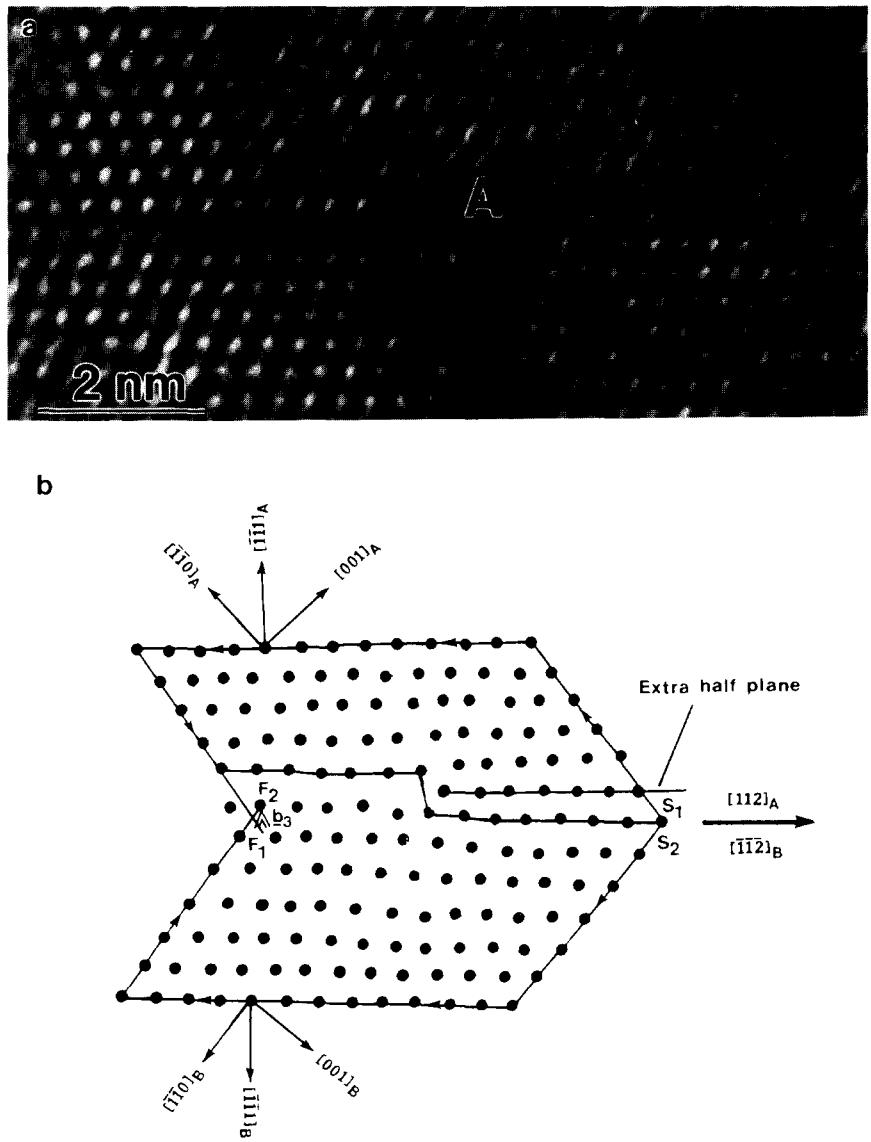

Fig. 6 (a) High-resolution image of side-step at twin boundary. (b) Schematic of (a). S_1, S_2 and F_1, F_2 correspond to the start and finish sites of the Frank circuit, respectively. b_3 indicates the magnitude of the closure failure vector.

undergoing a sidestep along a direction which is normal to the grain boundary plane [15]. In fig. 6, the immediately neighboring twin boundary on the left side of the defect does not have the (111) atomic planes of the neighboring grains in defect coincidence. That is, the twin boundary in this portion is slightly deviated from its ideal orientation. The dislocation brings in the perfect twin boundary orientation by simply allowing the boundary to undergo a monolayer atomic stepping along the grain boundary normal, i.e. along [$\bar{1}$11]. As well as this sideways stepping in the twinned structure of the silicon flake, such a defect is likely to occur when some irregularity in the deposition of silicon atoms from the melt on the twinned growth tip result in slight misorientation in the boundary configurations.

4. Discussion

The precise regularity of the stacking fault and twins in fig. 5 suggests that they are simply continuations of events that occurred at a point of nucleation. This further suggests that, in any one cluster, a group of parallel twins was present at the point of origin of the cluster and that no further twinning occurred during growth of any one platelet. In subsequent branching, twinned crystals form on the external {111} planes of a platelet as in figs. 3 and 4 and these twins are necessarily cozonal [2,3]. There remains the question of the transfer of cozonal twinning to each successive divergent cluster. The precise origin of a given cluster is not easily recognized, but it is proposed that a new cluster originates as a twinned branch from one of the platelets of the previous decaying cluster. If the mechanism of branching is as in figs. 3 and 4, twins in the new cluster will necessarily be cozonal, as before.

Thus, the absence of twins on three of the four possible twinning planes can be accounted for if the nucleation of twins does not occur during growth of the eutectic silicon except by the branching mechanisms of figs. 3 and 4. Twin nucleation occurs only during nucleation of silicon crystals at the point of origin of eutectic growth. A mechanism of nucleation which produces only cozonal twins has been observed [16]. The twins in the nucleus can then be transmitted through successive radiating clusters of silicon platelets as proposed above.

Acknowledgements

This work was carried out at the National Facility for High Resolution Electron Microscopy in the Center for Solid State Science of Arizona State University, supported by National Science Foundation Grant DMR-86-11609. We are pleased to acknowledge financial support from the US Department of Energy under contract DE-FG02-87ER42585.

References

[1] M.G. Day and A. Hellawell, Proc. Roy. Soc. (London) A305 (1968) 473.
[2] K. Kobayashi, P.H. Shingu and R. Ozaki, in: Proc. Sheffield Intern. Conf. on Solidification Casting (Metals Society, London, 1979) pp. 101–103.
[3] M. Shamsuzzoha and L.M. Hogan, J. Crystal Growth 76 (1986) 429.
[4] Shu-Zu Lu and A. Hellawell, Met. Trans. A18 (1987) 1721.
[5] R.S. Wagner, Acta Met. 8 (1960) 57.
[6] D.R. Hamilton and R. Seidensticker, J. Appl. Phys. 31 (1980) 1165.
[7] M. Shamsuzzoha and L.M. Hogan, Phil. Mag. A54 (1986) 459.
[8] Shu-Zu Lu and A. Hellawell, J. Crystal Growth 73 (1986) 316.
[9] D. Brooksbank and K.W. Andrews, J. Iron Steel Inst. 207 (1969) 474.
[10] A. Olson and J.C. Spence, Phil. Mag. A43 (1981) 945.
[11] W. Bollmann, Crystal Defects and Crystalline Interfaces (Springer, Berlin, 1979).
[12] M.L. Kronberg and F.M. Wilson, Trans. AIME 85 (1964) 26.
[13] R.W. Balluffi, in: Interfacial Segregation (Am. Soc. Metals, Metals Park, OH, 1979).
[14] D.A. Smith and R.C. Pond, Intern. Met. Rev. 205 (1976) 61.
[15] J.P. Hirth and R.W. Balluffi, Acta Met. 21 (1972) 929.
[16] K. Kobayashi and L.M. Hogan, Phil. Mag. A40 (1979) 399.